

Three-dimensional simulations of solar wind turbulence with the hybrid code CAMELIA

L. Franci¹, P. Hellinger², M. Guarrasi³, C. H. K. Chen⁴, E. Papini¹, A. Verdini¹, L. Matteini⁵, and S. Landi^{1,6}

¹Dipartimento di Fisica e Astronomia, Università degli Studi di Firenze, Firenze, Italy

²Astronomical Institute, CAS, Prague, Czech Republic

³SuperComputing Applications and Innovation Department, CINECA, Bologna, Italy

⁴School of Physics and Astronomy, Queen Mary University of London, London, UK

⁵LESIA-Observatoire de Paris, Meudon, France

⁶INAF - Osservatorio Astrofisico di Arcetri, Firenze, Italy

E-mail: franci@arcetri.astro.it

Abstract. We investigate the spectral properties of plasma turbulence from fluid to sub-ion scales by means of high-resolution three-dimensional (3D) numerical simulations performed with the hybrid particle-in-cell (HPIC) code CAMELIA. We produce extended turbulent spectra with well-defined power laws for the magnetic, ion bulk velocity, density, and electric fluctuations. The present results are in good agreement with previous two-dimensional (2D) HPIC simulations, especially in the kinetic range of scales, and reproduce several features observed in solar wind spectra. By providing scaling tests on many different architectures and convergence studies, we prove CAMELIA to represent a very efficient, accurate and reliable tool for investigating the development of the turbulent cascade in the solar wind, being able to cover simultaneously several decades in wavenumber, also in 3D.

1. Introduction

Turbulence in magnetized collisionless plasmas, such as the solar wind, is one of the major challenges of space physics and astrophysics. Both the anisotropic flow of energy toward smaller scales (cascade) and the damping of energy at dissipative scales are poorly understood. Solar wind turbulent fluctuations are generated at large magneto-hydrodynamic (MHD) scales and dissipated at scales where particle kinetics dominates. Indeed, in situ measurements show spectra of the plasma and electromagnetic fields with a power-law scaling spanning several decades in frequency, with a spectral break in the magnetic and density spectrum at proton scales, separating the MHD inertial range cascade from a second power-law interval at kinetic scales (see [1] for a recent summary). A further change in the spectral properties occurs at the electron scales, although distinguishing between an exponential cut-off [2] or a power law [3] is not straightforward and thus no universal behavior is observed.

Very large numerical resources are required to investigate the whole turbulent cascade, since at least two full decades in wavevectors across the transition needs to be covered simultaneously. Full Particle-In-Cell (PIC) simulations represent the most comprehensive numerical tool for simulating the plasma dynamics up to electron spatial and temporal scales, e.g., [4, 5, 6, 7, 8, 9, 10, 11, 12, 13]. However, due to computational limitations, they typically employ a limited accuracy (e.g., small resolution, small number of particles, small ion-to-electron mass ratio).

Run	Grid	Δx	$L [d_i]$	$\mathbf{B}^{\text{rms}}/B_0$	$k_0 d_i$	$k_{\text{inj}} d_i$	ppc
A	512^3	0.25	128	0.40	0.05	0.25	2048
B	256^3	0.25	64	0.38	0.10	0.30	2048
C	256^3	0.25	64	0.38	0.10	0.30	1024
D	256^3	0.25	64	0.38	0.10	0.30	512
E	2048^2	0.125	256	0.24	0.025	0.28	8000

Table 1. List of simulations and their main different parameters

Alternatively, reduced models have been largely used in the last decade to simulate plasma turbulence at kinetic scales, both in 2D and 3D, e.g., Hall-MHD [14, 15, 16, 17, 18], Electron-MHD [19, 20, 21], Gyrokinetic [22, 23, 24, 25], finite Larmor radius-Landau fluid [26, 27, 28], hybrid Vlasov-Maxwell [29, 30, 31, 32, 33, 34, 35, 36], and Hybrid Particle-In-Cell (HPIC) [37, 38, 39, 40, 41, 42, 43, 44, 45].

In particular, very high-resolution 2D simulations, performed with the HPIC code CAMELIA, recently fully covered the transition between fluid and kinetic scales [46, 47, 48]. Moreover, they produced extended turbulent spectra with well-defined power laws for the plasma and electromagnetic fields, in agreement with solar wind observations. Such results have been recently extended to 3D [49].

2. Numerical setup

The simulations presented here have been performed using the 3D HPIC code CAMELIA (see Sec. 5 for details). The characteristic spatial unit is the ion (proton) inertial length, $d_i = v_A/\Omega_i$, v_A being the Alfvén speed, while the temporal unit is the inverse ion gyrofrequency, $1/\Omega_i$. We compare four simulations, all employing a periodic cubic grid with spatial resolution $\Delta x = 0.25 d_i$, with two different numbers of grid points (512^3 and 256^3) and, consequently, two different box sizes ($L_{\text{box}} = 128 d_i$ and $64 d_i$), and with three different numbers of (macro)particle-per-cell, ppc, representing protons (512, 1024, and 2048). In all four cases, the equilibrium system is a homogeneous plasma, with uniform density and temperature, embedded in a mean magnetic field, \mathbf{B}_0 . The plasma beta, i.e., the ratio of the plasma pressure to the magnetic pressure, is $\beta = 0.5$ for both the protons and the electrons. This system is perturbed with magnetic and ion bulk velocity fluctuations, purely perpendicular to \mathbf{B}_0 , consisting of a superposition of Fourier modes of equal amplitude and random phases in the range $k_0 < k < k_{\text{inj}}$ ($k = \sqrt{k_x^2 + k_y^2 + k_z^2}$). The minimum wavenumber, $k_0 = 2\pi/L_{\text{box}}$, is $0.05 d_i^{-1}$ for the large box and $0.10 d_i^{-1}$ for the small one, while the maximum injection scale is $k_{\text{inj}} = 0.25 d_i^{-1}$ and $0.30 d_i^{-1}$, respectively. A more detailed description of the initialization and of the physical and numerical parameters can be found in [46, 47]. The main differences between the four 3D simulations are summarized in Tab. 1 (runs A-D), where we also recall the parameters of a 2D HPIC simulation with the same β (run E), presented in [46, 47].

3. Results

We start with the results of run A, already presented in [49], focusing on the spectral properties of th electromagnetic and plasma fluctuations at the time when the turbulent cascade has fully developed. For the definitions of the 1D omnidirectional spectra, P_{1D} , the 1D reduced perpendicular and parallel spectra with respect to the global mean field \mathbf{B}_0 , $P_{1D,\perp}$ and $P_{1D,\parallel}$, and for the description of the filtering procedure used to obtain them from the 3D power spectra, please refer to [49].

In the top panels of Fig. 1, we show a comprehensive overview of the 1D omnidirectional power spectra of all fields for the 3D run A (left), to be compared with the results of the 2D run E [46, 47] (right). Additionally, characteristic power laws are drawn with dashed black lines as reference. The main

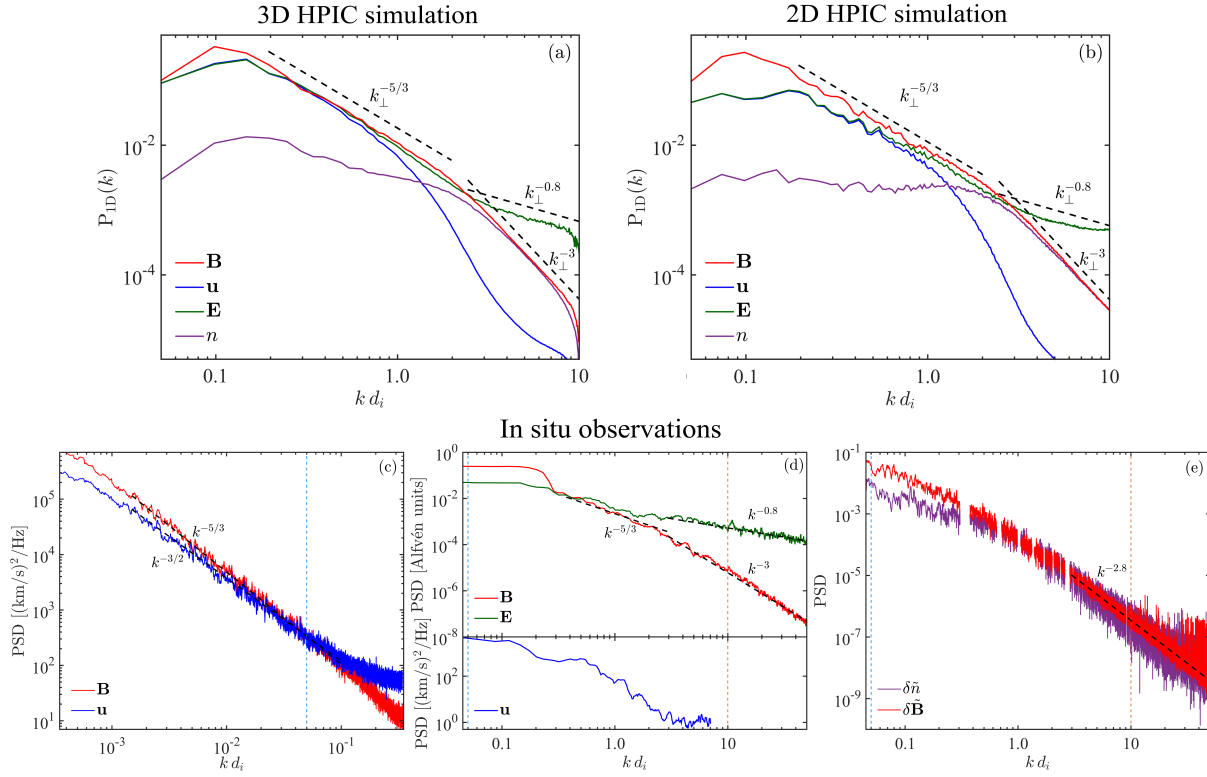


Figure 1. Qualitative comparison of the 1D omnidirectional spectra of the magnetic field (red), ion bulk velocity (blue), electric field (green), and density (purple) between the 3D run A and the 2D run E (panels (a) and (b), respectively). Additionally, the bottom panels show results of solar wind and magnetosheath observations from [50] (c), [51] (d), and [52] (e). A light blue and an orange dashed lines mark the smaller and larger wavenumbers covered by the 3D HPIC simulation, respectively.

similarities between the 3D and the 2D cases are: (i) the double power-law behavior of the magnetic fluctuations, with a spectral index close to $-5/3$ at MHD scales and a steepening (~ -3) at sub-ion scales, (ii) the strong coupling between magnetic and density fluctuations at sub-ion scales, with the same amplitude and similar slopes, (iii) the flattening of the electric field spectrum in the kinetic range, with a spectral index close to -0.8 , (iv) the sharp decline of the ion bulk velocity spectrum, which quickly reaches the noise level. All these features are in broad agreement with solar wind observations [50, 51, 52], as shown in the bottom panels of Fig. 1, where a light blue and an orange dashed lines mark the smaller and larger wavenumbers covered by the 3D HPIC simulation, respectively. On the contrary, differences arise at MHD scales for the velocity, electric field, and density spectra. In particular, in the 3D case the magnetic and velocity fluctuations are more strongly coupled, since they are almost equal amplitude, in Alfvén units, up to $kd_i \lesssim 1$. A higher level of density fluctuations is also observed. Unexpectedly, a better agreement is recovered between observations and the 2D simulation for what concerns the ion bulk velocity spectrum. The latter exhibits a lower level of fluctuations than the 3D case, and therefore a sizeable residual energy (difference between magnetic and kinetic energy). This discrepancy between 2D and 3D might be due to the different geometry or to the different setting, e.g., to the initial level of fluctuations or resolution (see Tab. 1). Indeed, the 3D physical domain is a factor of 2 smaller than the 2D one and this, and this might constrain the dynamics at the largest scales.

In Fig. 2, we show in separate panels the 1D omnidirectional spectra of the magnetic field, \mathbf{B} (top left), ion bulk velocity, \mathbf{u} (top right), electric field, \mathbf{E} (bottom left), and density, n (bottom right) for run A.

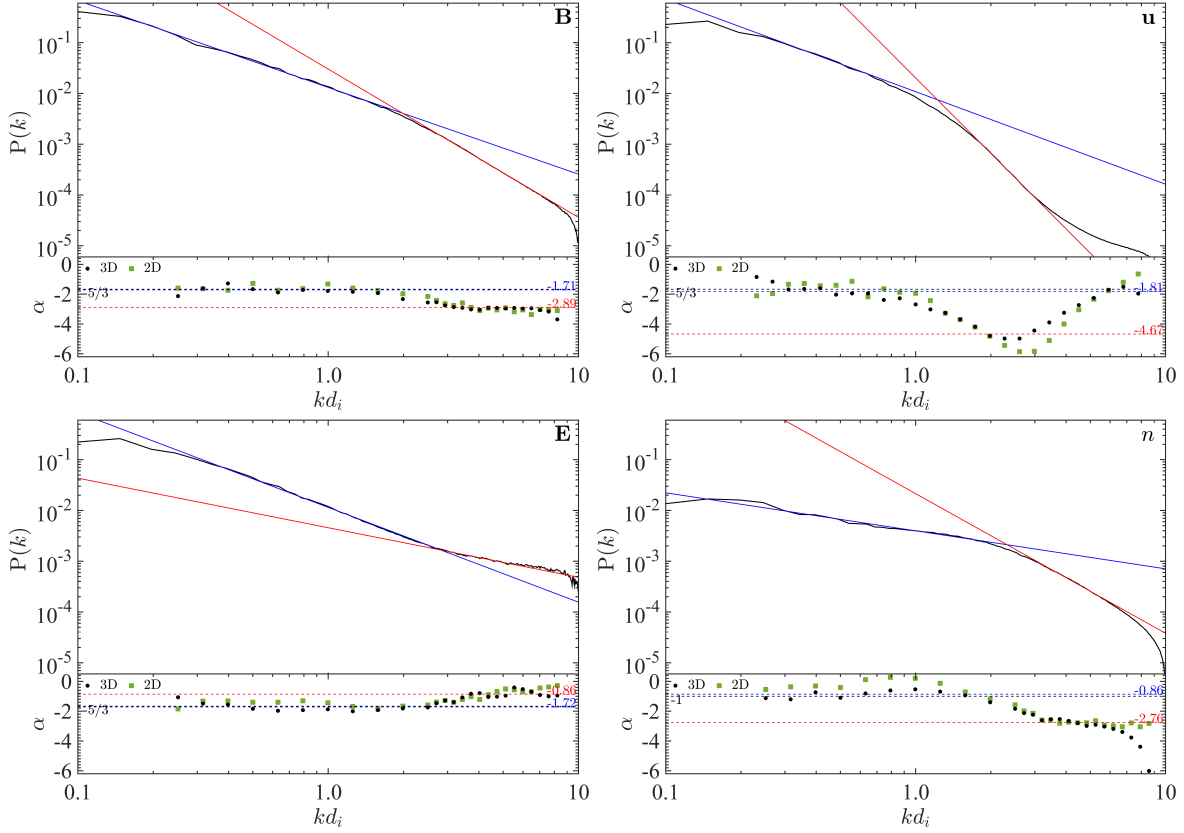


Figure 2. 1D omnidirectional power spectra of the magnetic field (top left), ion bulk velocity (top right), electric field (bottom left), and density (bottom right) for run A. Power-law global fits are reported for the MHD range (blue) and the kinetic range (red). In the bottom region of each panel, the value of the local spectral index, α (black), is compared with the results of the two global fits in corresponding colors and with the local spectral index of the 2D run E (green).

We fit each spectrum with two power laws, one the MHD range (blue straight line) and one in the kinetic range (red), as already done for 2D HPIC simulations [48]. Additionally, we perform local power-law fits over many small intervals in the range $k_{\perp}d_i \in [0.25, 10]$. The values of the local spectral index, α , are shown with black dots in the bottom part of each panel. Two horizontal dashed lines represent the slopes of the two global fits, with the respective colors. We also directly compare α for the 3D run A (black) and the 2D run E (green).

The magnetic field spectrum exhibits two clear power-law intervals spanning almost two decades in wavevector, with a spectral index of $\sim -5/3$ and ~ -2.9 at MHD and sub-ion scales, respectively, and a transition at $kd_i \gtrsim 2$. The velocity spectrum shows a power-law-like behaviour at large scales, although less extended than the magnetic field's, with a spectral index close to $-5/3$ in 3D and slightly closer to $-3/2$ in 2D. For $kd_i \gtrsim 1$, the spectrum drops very rapidly, reaching the ppc noise level at slightly smaller scales. The hint of a power-law shape can be inferred, significantly steeper than the magnetic field's. However, the small extent in k prevents us from providing either a clear evidence of a power law with respect to an exponential drop, nor a common value of the slope between the 3D and the 2D runs. The electric field spectrum shows an extended Kolmogorov-like power law at MHD scales and flattens toward a spectral index of ~ -0.8 around ion scales, consistently with the generalized Ohm's law [47]. Finally, the density spectrum is almost flat at intermediate scales, with a slope ~ -0.9 , although it seems

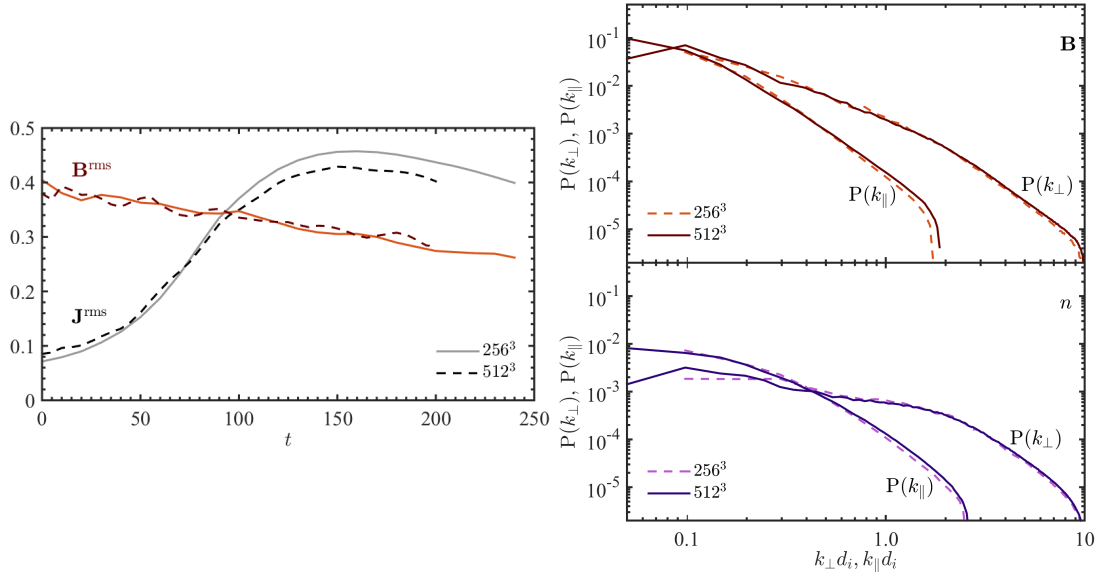


Figure 3. Comparison between run A and B, employing different numbers of grid points. Left panel: time evolution of rms of the magnetic field, B^{rms} and of current density, J^{rms} . Right panels: 1D reduced perpendicular and parallel spectra of the magnetic (red, top) and density (purple, bottom) fluctuations.

to be slightly steeper at the largest scales. A transition is clearly observed around ion scales, followed by a power law with a spectral index of ~ -2.7 .

4. Role of numerical parameters

A very high accuracy is required to investigate the turbulent cascade from large MHD scales to small kinetic ones. In particular, in order to quantitatively compare numerical results with solar wind observations (e.g., the spectral indices of electromagnetic and plasma fluctuations and the scale of the MHD-kinetic spectral break) one needs to cover simultaneously at least two full decades in wavevectors across the transition. Moreover, artificial effects due to the finite spatial resolution, the finite box size and the finite number of particles have to be carefully checked, so that the numerical results can be considered robust and reliable. While all this has been feasible in 2D in recent years [47], it is not trivial in 3D. Here we provide such an analysis, in support of the results recently presented in [49].

4.1. Box size

We investigate the effects of the box size by running two simulations with the same setting and numerical parameters, except for different grid sizes, 512^3 (run A) and 256^3 (run B). Consequently, the box size changes from $128 d_i$ to $64 d_i$. The left panel of Fig. 3 shows that the use of a smaller box does not affect considerably the time evolution of the system. The rms value of the magnetic fluctuations, B^{rms} (red line), exhibits very small variations around the same average value, with the same slow decrease, while the rms of the current density, J^{rms} (black), shows the very same behavior up to $t \sim 100$ but then it reaches a slightly smaller peak value. This difference is mainly due to the fact that for run B the same resistivity as for run A was set, while it should be slightly decreased in order to take into account the small increase in the minimum wavenumber and in the injection scale. In the right panel of Fig. 3, we also compare the reduced perpendicular and parallel spectra of the total magnetic fluctuations (top) and the density fluctuations (bottom) between runs A and B. The differences in $P_{1D,\perp}^B$ and $P_{1D,\perp}^n$ are indeed negligible. Even $P_{1D,\parallel}^B$ and $P_{1D,\parallel}^n$ show no significant differences, except for a very small deviation at the smallest parallel scales, that are not suppressed by the filtering procedure, i.e., for $k_{\parallel} d_i \gtrsim 1$.

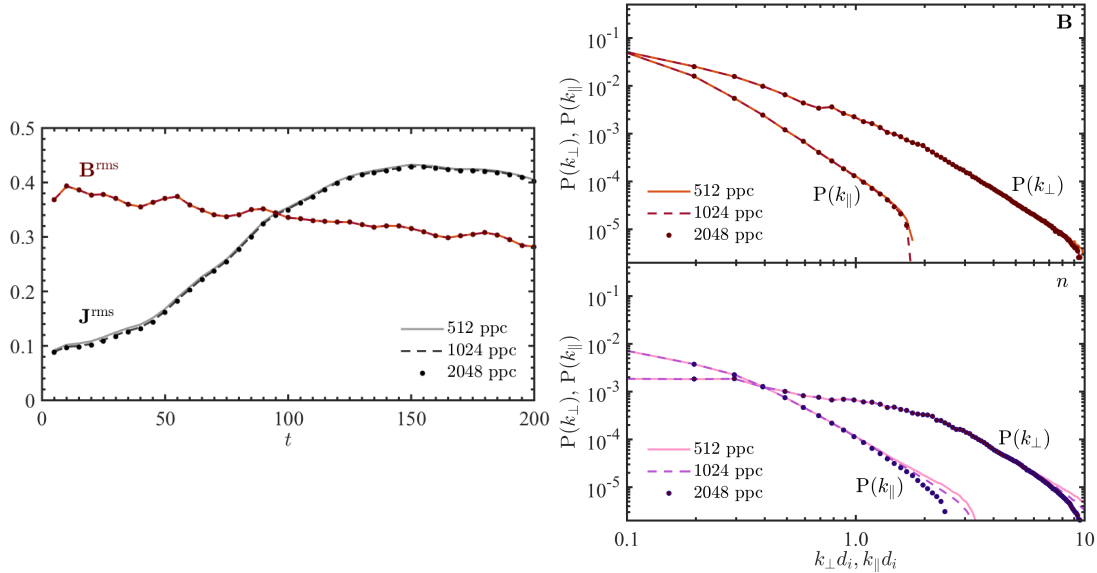


Figure 4. The same as in Fig. 3, but for the comparison between run B, C, and D, employing different numbers of ppc.

4.2. Number of particles (ppc)

We investigate the effects of the number of particles, in order to determine the optimal number which allows for obtaining reliable results at sub-ion scales. We use two simulations employing the small box and the same parameters as in run B, except for different numbers of ppc, i.e., 1024 (run C) and 512 (run D) instead of 2048. The left panel of Fig. 4 shows that the use of fewer particles, at least a factor of 4, has no effect on the evolution of global quantities: both B^{rms} and J^{rms} exhibit the same behavior over time. The same consideration holds for the spectral properties of the magnetic fluctuations (top right panel of Fig. 4). The only, almost negligible, differences arise in $P_{1D,\perp}^n$ (bottom right) at the scales corresponding to the grid spacing and, correspondingly, in $P_{1D,\parallel}^n$ at scales $k_{\parallel} d_i \gtrsim 1$. Note that the filtering procedure already removes most of the artificial features due to the noise, making the use of a very large number of ppc unnecessary. As a consequence, for an intermediate-beta case such as the one presented here, 512 ppc could be already enough in order to investigate the development of the kinetic cascade and the spectral properties. However, if one intends to investigate the evolution of the proton temperature (not discussed here), the use of a larger number of ppc would likely be advisable, as previously shown in 2D [47].

5. The hybrid particle-in-cell (HPIC) code CAMELIA

5.1. Overview and applications

CAMELIA¹ (Current Advance Method Et cycLIc leApfrog) is a HPIC code, where the electrons are considered as a massless, charge neutralizing fluid, whereas the ions are described as macroparticles, i.e., statistically-representative portions of the distribution function in the phase space. Up to 2016, the code was only parallelized through the Message Passing Interface (MPI) Library using spatial and/or particle decompositions, with the former being available in all spatial directions. In early 2017, a hybrid parallelization using both MPI and the Open MultiProcessing (OpenMP) Interface has been implemented, which fully exploits the latest architectures for High Performance Computing, including many-integrated cores Intel Knights Landing processors. Different formats can be chosen for the

¹ Official CAMELIA website: <http://terezka.asu.cas.cz/helinger/camelia.html>

output files, i.e., ASCII, binary, or HDF5, including parallel binary (MPI-IO) and parallel HDF5. A checkpoint/restart procedure is implemented, with a HDF5 file written by each MPI process, assuring a wide portability across different platforms. The boundary conditions are periodic in all directions. Alternatively, in 2D, one can choose reflecting boundary conditions on one side and open boundary conditions, with a continuous injection of particles, on the other side (e.g., allowing for the generation of shock waves).

CAMELIA has two major extensions, being able to model (i) the effects of a slow expansion, using the Hybrid Expanding-Box (HEB) model (Hellinger et al., 2003; Hellinger and Travnicek, 2005), and (ii) the effects of Coulomb collisions, using the Langevin representation (Hellinger and Travnicek, 2010, 2015). In the last decade, it has been extensively used to investigate the spectral and heating properties of solar wind turbulence from MHD to sub-ion scales in 2D [46, 47], recovering a good agreement with solar wind observations. Such findings have also been validated by comparing with the results obtained by numerical simulations performed with the Eulerian hybrid Vlasov-Maxwell code HVM [53]. A particular focus has been devoted to the correlation between vorticity and proton temperature [54], to the dependence of the ion-scale spectral break on the plasma beta [48], and to the role of magnetic reconnection as a trigger for the sub-ion scale cascade [55]. The study of the spectral behavior of electromagnetic and plasma fluctuations has recently been extended to 3D [49]. Furthermore, the coexistence of kinetic instabilities with strong plasma turbulence has been investigated by means of 2D HEB simulations including the effects of the solar wind expansion [42, 56].

5.2. Numerical scheme

CAMELIA is based on the Current Advance Method and Cyclic Leapfrog (CAM-CL) code of Matthews [57]. The system is governed by the Vlasov-fluid equations, comprising the equations of motions for individual ions, and the electron fluid equations. The ions are described by a PIC model, a technique used to solve a certain class of partial differential equations where particles (or fluid elements) in a Lagrangian frame are tracked in continuous phase space, whereas moments of the distribution such as densities and currents are computed simultaneously on Eulerian (stationary) mesh points. The central engine of the code is a CAM-CL algorithm, which integrates the differential equations in a manner that is explicit in time and spatially local. The plasma has two time-independent components: ion macro-particles with position and velocities and the magnetic field specified at the nodes of a regular computing grid. The displacement current is neglected in Maxwells equations, so there is no equation for the time-evolution of the electric field, which is just a function of the ion moments (interpolated at grid points from particle data), the magnetic field, and the electron temperature. (Bi, tri)linear interpolation is used for moment collection and evaluation of the Lorentz force at particle positions. An explicit form of the time-dependent differential equation is used. A CAM method is used to advance the ion current density. The original leapfrog particle advance has been replaced by the more precise Boris' algorithm [58], which has been proved to have an excellent long-term accuracy [59]. This requires the fields to be known at half time step ahead of the particle velocities, which is achieved by advancing the current density to this time step, with only one computational pass through the particle data at each time step (see Fig. 5). Cyclic leapfrog is used to advance the magnetic field with a sub-stepping using two copies of the magnetic field.

5.3. Performance

CAMELIA has been optimized and run on many thousands of cores on High Performance Computing (HPC) systems with different architectures. Here we provide scaling tests performed on:

- SuperMike-II (Intel Sandy Bridge) @ Louisiana State University, Baton Rouge, U.S. (2015)
- Fermi (IBM Blue Gene/Q) @ CINECA, Bologna, Italy (2016)
- Cartesius (Intel Haswell) @ SURFsara, Amsterdam, The Netherlands (2017)

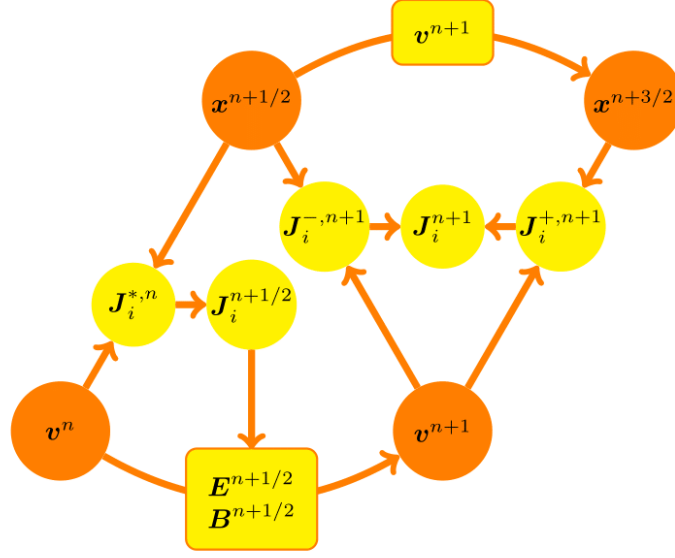


Figure 5. Schematic diagram of the code CAMELIA. The particle positions and velocities are taken at the different times, separated by half the (particle) time step $\Delta t/2$, \mathbf{v}^n and $\mathbf{x}^{n+1/2}$, where the subscript n refers to time t and $n + 1/2$ to time $t + \Delta t/2$. At the beginning, there are the current density, $\mathbf{J}_i^{n+1/2} = \mathbf{J}(\mathbf{x}^{n+1/2})$, and the “free-streaming” ionic current, $\mathbf{J}_i^{*,n} = \mathbf{J}_i(\mathbf{x}^{n+1/2}, \mathbf{v}^n)$, as well as $\mathbf{J}^n = \mathbf{J}_n(\mathbf{x}_n)$ and $\mathbf{J}_i^n = \mathbf{J}_i(\mathbf{x}_n, \mathbf{v}_n)$. The magnetic field is advanced (using two copies via cyclic leapfrog) from \mathbf{B}_n to $\mathbf{B}^{n+1/2}$ with $\mathbf{E}(\mathbf{J}^n, \mathbf{J}_i^n, \mathbf{B})$. The Current Advance Method advances $\mathbf{J}_i^{*,n}$ to $\mathbf{J}_i^{n+1/2}$. Using $\mathbf{B}^{n+1/2}$ and $\mathbf{E}^{n+1/2} = \mathbf{E}(\mathbf{J}^{n+1/2}, \mathbf{J}_i^{n+1/2}, \mathbf{B}^{n+1/2})$, the particles are advanced using the Boris’ scheme to \mathbf{v}^{n+1} and $\mathbf{x}^{n+3/2}$ and moments are collected, $\mathbf{J}^{n+3/2} = \mathbf{J}(\mathbf{x}^{n+3/2})$; \mathbf{J}^{n+1} is obtained as an average of $\mathbf{J}^{n+1/2}$ and $\mathbf{J}^{n+3/2}$. Forward and backward “free-streaming” ionic currents, $\mathbf{J}_i^{-,n+1} = \mathbf{J}_i(\mathbf{x}^{n+1/2}, \mathbf{v}^{n+1})$ and $\mathbf{J}_i^{+,n+1} = \mathbf{J}_i(\mathbf{x}^{n+3/2}, \mathbf{v}^{n+1})$, are collected and their average give \mathbf{J}_i^{n+1} . Finally, $\mathbf{B}^{n+1/2}$ is advanced to \mathbf{B}^{n+1} .

	Peak Performance	Clock	Cores/node	RAM/node	Network
SuperMike-II	146 TFlops	2.6 GHz	16	32 GB	40 Gbit/s Infiniband
Fermi	2 PFlops	1.6 GHz	16	16 GB	5D Torus
Cartesius	1.8 PFlops	2.6 GHz	24	64 GB	100 Gbit/s Infiniband
Marconi-A1	2 PFlops	2.3 GHz	36	128 GB	Intel OmniPath
Marconi-A2	11 PFlops	1.4 GHz	68	16+96 GB	Intel OmniPath

Table 2. Main parameters of the different HPC systems used for scaling tests

- Marconi-A1 (Intel Broadwell) @ CINECA, Bologna, Italy (2017)
- Marconi-A2 (Intel Knights Landing) @ CINECA, Bologna, Italy (2017)

The main features of these HPC systems are summarized and compared in Tab. 2.

For all systems, we performed test simulations with seven different problem sizes (three for each machine) for measuring the strong-scaling performances and four different sizes (one or more for each machine) for the weak scaling (see Fig. 6- 10). In CAMELIA, we evolve more than 30 different field components (taking into account both physical variables and additional temporary auxiliary grid variables), plus the 3 position components and the 3 velocity components of each particle. Since we always put thousands of particles in each grid cell, the particles positions and velocities represent the dominant contribution to the memory requirement, which is of the order of 4 Bytes (single precision)

Size	Particles	RAM	Color
XS	$\sim 2.1 \times 10^9$	48 GB	violet
S	$\sim 8.6 \times 10^9$	192 GB	indigo
M	$\sim 1.7 \times 10^{10}$	384 GB	blue
L	$\sim 3.4 \times 10^{10}$	768 GB	green
XL	$\sim 6.7 \times 10^{10}$	1.5 TB	yellow
XXL	$\sim 1.4 \times 10^{11}$	3.0 TB	orange
XXXL	$\sim 2.7 \times 10^{11}$	6.0 TB	red

Table 3. Problem sizes for strong scaling tests

$\times 6$ variables \times number of ppc \times number of cells. In Tab. 3, we list all the different problem sizes, indicating the total number of particles in the whole simulation domain and the corresponding total memory requirement. A color has been associated to each problem size, so that a qualitative comparison of code performances for a fixed sized between different machines can be easily done by eye. Note that the same global size can result from different configurations, i.e., number of grid points \times number of ppc. These are explicitly indicated in the legend of each plot.

In Fig. 6-10, we report all the scaling tests that we performed on the above mentioned systems, both for strong scaling (left panels) and weak scaling (right panels), versus the number of cores. Until 2016, only a pure MPI parallelization was implemented, so the number of cores for SuperMike-II, Fermi, Cartesius and Marconi-A1 also corresponds to the number of MPI processes. Since early 2017, a hybrid MPI+OpenMP version is also available, allowing us to fully exploit the Intel Many Integrated Core Architecture. Test simulations on Marconi-A2 were run with 32 MPI processes per node, i.e., half the number of cores per node (since 4 over 68 were left available for the operating system and I/O operations) and 8 OpenMP threads per MPI task. Therefore, the code scalability has been measured up to 16384 MPI tasks \times 8 OpenMP threads/MPI task = 131072 total threads.

Fig. 6-10 show that both the strong and the weak scalability are quite good in all the analyzed architectures. In particular, the weak scalability is very promising. The parallel efficiency on standard Intel x86 architectures is near to 1 at least up to 2048 cores. Both in the Haswell and Broadwell cases (Cartesius and Marconi-A1) this efficiency is also slightly greater than 1, and this is probably due to a more optimal use of the memory with an high number of cores. Furthermore, the weak scalability on Blue Gene/Q architectures is also more promising. Indeed, in almost all the analyzed cases (with the exception of the smallest one) the parallel efficiency is near to 1 at least up to 8192 cores. This increase of parallel performance is likely due to a combination of factors, the most important ones being the high speed Torus 5D Blue Gene/Q network and the ratio between the network (and memory, of course) bandwidth and the CPU clock. The weak scaling tests on F also clearly show that, for the same problem size, CAMELIA is more efficient in running 3D simulations than 2D, due to the more favorable ratio between computations and communications when parallelizing the computational domain into cubes instead of rectangles. Finally for what concerns the parallel performances on KNL machines, the weak parallel efficiency is close to 1, as expected, up to 4096 cores (i.e. the same number of nodes as in the Broadwell case), which correspond to 16384 total OpenMP threads, while it is lower for larger number of cores, mainly due to the fact that a smaller workload per core has been employed.

Size	Particles/MPI	RAM/MPI	Color
S	$\sim 4.2 \times 10^7$	96 MB	indigo
M	$\sim 1.7 \times 10^7$	384 MB	blue
L	$\sim 3.4 \times 10^7$	768 MB	green
XL	$\sim 6.7 \times 10^7$	1.5 GB	yellow

Table 4. Problem sizes for weak scaling tests

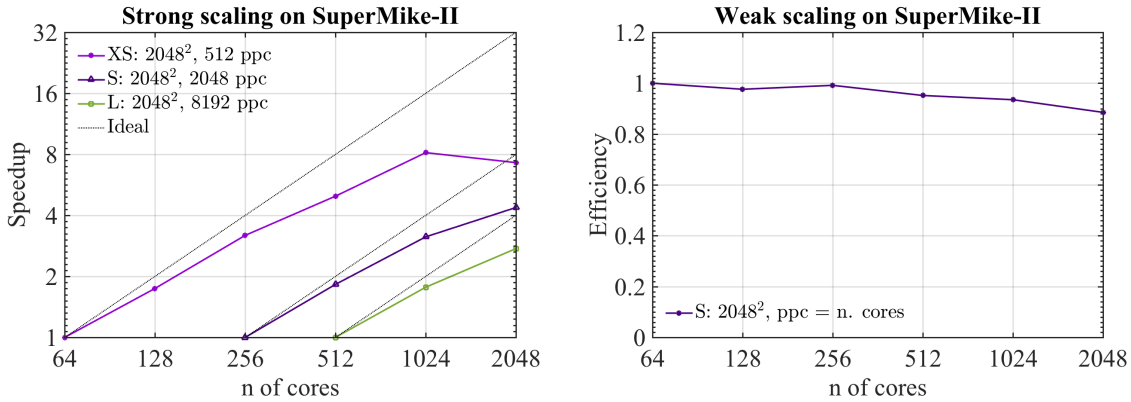


Figure 6. Code performances of CAMELIA’s pure MPI version on the Sandy Bridge architecture, i.e., “SuperMike-II”: strong scaling (left panel) and weak scaling tests (right panel).

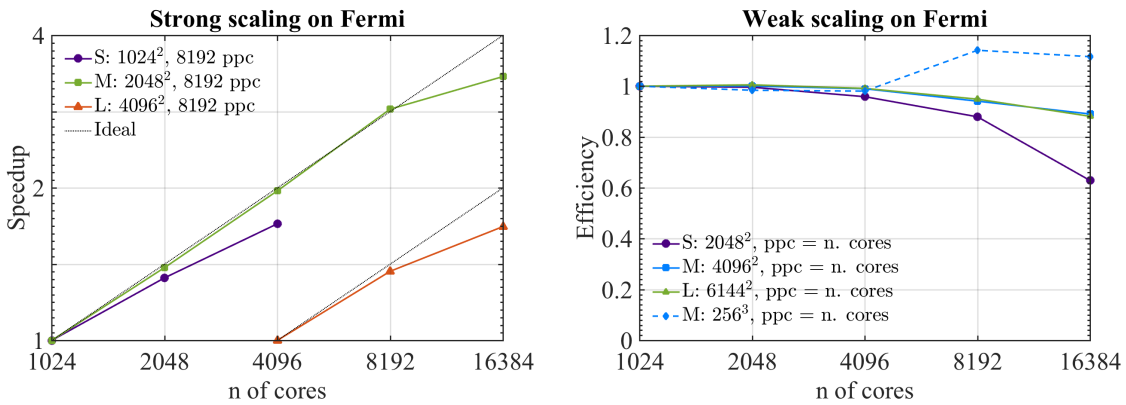


Figure 7. The same as in Fig. 6, but for an IBM Blue Gene/Q architecture, i.e., “Fermi”.

6. Conclusions

CAMELIA is a 3D hybrid kinetic numerical code, suitable for investigating the development of plasma turbulence and its interplay with kinetic instabilities over a wide range of scales. Indeed, it allows for the simultaneous modelling of the MHD and the sub-ion-scale dynamics, fully capturing the transition between the two regimes. Being highly performing on many different HPC systems, CAMELIA allows us to perform state-of-the-art 2D HPIC simulations in a walltime of a few hours and 3D HPIC simulations within a day. In the last few years, the results of the HPIC simulations performed with the code CAMELIA showed a remarkable agreement with solar wind observations, both in 2D and 3D.

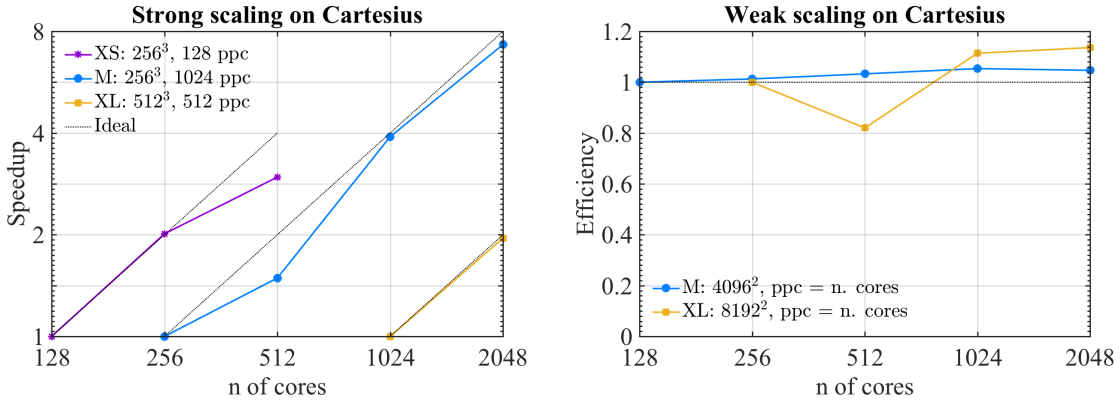


Figure 8. The same as in Fig. 6, but for an Intel Hashwell architecture, i.e., “Cartesius”.

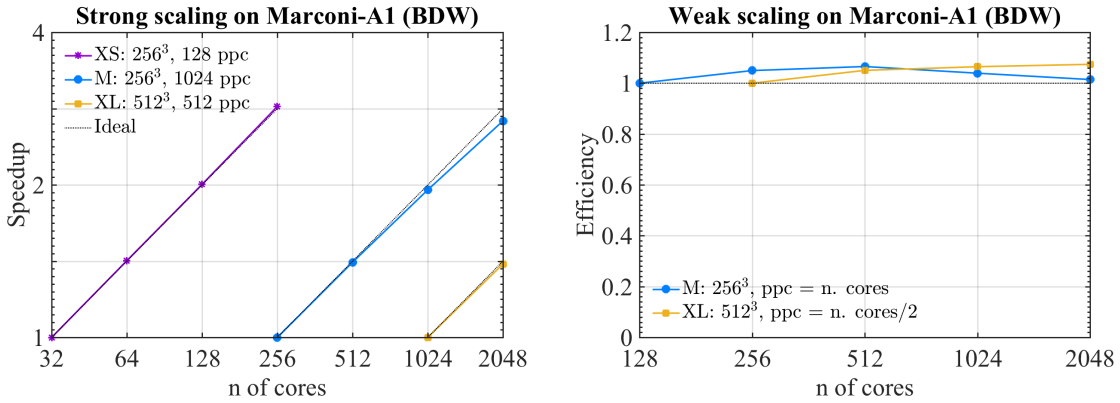


Figure 9. The same as in Fig. 6, but for an Intel Broadwell architecture, i.e., “Marconi-A1 (BDW)”.

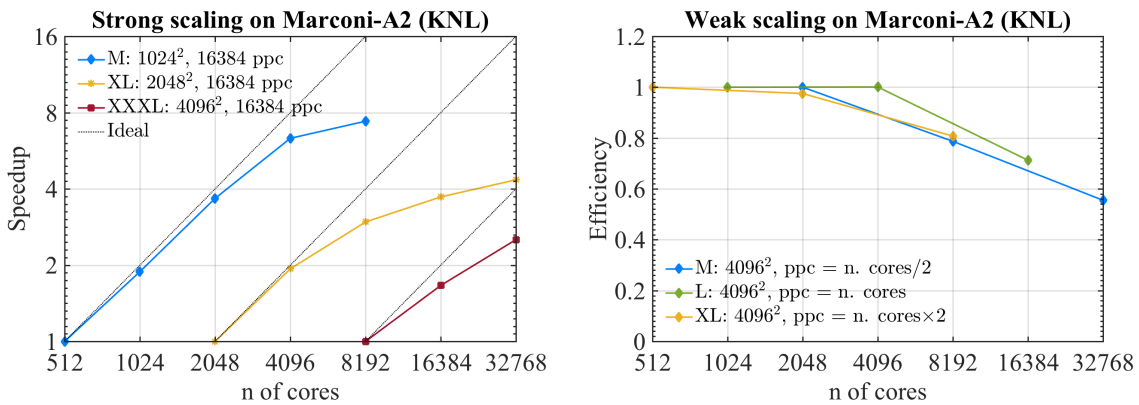


Figure 10. Code performances of CAMELIA’s hybrid MPI+OpenMP version on an Intel Knights Landing architecture, i.e., “Marconi-A2”.

As far as 3D simulations are concerned, we showed that a 256³ computational domain with a spatial resolution of $d_i/4$ and 512 particle-per-cell may be accurate enough for investigating the development of

the turbulent cascade simultaneously from MHD to sub-ion scales in an intermediate- or small-beta plasma. This “reduced” setting can therefore be safely employed for future parameter studies and convergence studies in three dimensions. However, based on [47, 48], we can reasonably expect that a larger number of particles would be mandatory for properly investigating the evolution of the proton temperature, or the spectral properties in systems with $\beta \gtrsim 1$.

7. Acknowledgments

The authors thank T. Tullio for useful comments and suggestions. LF is funded by Fondazione Cassa di Risparmio di Firenze through the project “Giovani Ricercatori Protagonisti”. PH acknowledges GACR grant 15-10057S. CHKC is supported by an STFC Ernest Rutherford Fellowship. We acknowledge PRACE for awarding us access to resource Cartesius based in the Netherlands at SURFsara through the DECI-13 (Distributed European Computing Initiative) call (project HybTurb3D), and the CINECA award under the ISCRA initiative, for the availability of high performance computing resources and support (grants HP10C877C4, HP10CVCUF1, HP10B2DRR4, HP10BUUOJM). We warmly thank Frank Löffler for providing HPC resources through the Louisiana State University (allocation hpc hyrel14). Data deposit was provided by the EUDAT infrastructure (<https://www.eudat.eu/>).

References

- [1] Chen C H K 2016 *Journal of Plasma Physics* **82** 535820602
- [2] Alexandrova O, Lacombe C, Mangeney A, Grappin R and Maksimovic M 2012 *Astrophys. J.* **760** 121
- [3] Sahraoui F, Huang S Y, Belmont G, Goldstein M L, Réтино A, Robert P and De Patoul J 2013 *Astrophys. J.* **777** 15
- [4] Svidzinski V A, Li H, Rose H A, Albright B J and Bowers K J 2009 *Phys. Plasmas* **16** 122310
- [5] Saito S, Gary S P and Narita Y 2010 *Phys. Plasmas* **17** 122316
- [6] Chang O, Gary P S and Wang J 2011 *Geophys. Res. Lett.* **38** L22102
- [7] Camporeale E and Burgess D 2011 *Astrophys. J.* **730** 114
- [8] Gary S P, Chang O and Wang J 2012 *Astrophys. J.* **755** 142
- [9] Wan M, Matthaeus W H, Karimabadi H, Roytershteyn V, Shay M, Wu P, Daughton W, Loring B and Chapman S C 2012 *Phys. Rev. Lett.* **109** 195001
- [10] Karimabadi H, Roytershteyn V, Wan M, Matthaeus W H, Daughton W, Wu P, Shay M, Loring B, Borovsky J, Leon2ardis E, Chapman S C and Nakamura T K M 2013 *Phys. Plasmas* **20** 012303
- [11] Wan M, Matthaeus W H, Roytershteyn V, Karimabadi H, Parashar T, Wu P and Shay M 2015 *Phys. Rev. Lett.* **114** 175002
- [12] Gary S P, Hughes R S and Wang J 2016 *Astrophys. J.* **816** 102
- [13] Wan M, Matthaeus W H, Roytershteyn V, Parashar T N, Wu P and Karimabadi H 2016 *Phys. Plasmas* **23** 042307
- [14] Shaikh D and Shukla P K 2009 *Phys. Rev. Lett.* **102** 045004
- [15] Shaikh D and Zank G P 2009 *MNRAS* **400** 1881–1891
- [16] Martin L N, De Vita G, Sorriso-Valvo L, Dmitruk P, Nigro G, Primavera L and Carbone V 2013 *Phys. Rev. E* **88** 063107
- [17] Rodriguez Imazio P, Martin L N, Dmitruk P and Mininni P D 2013 *Phys. Plasmas* **20** 052506
- [18] Gómez D, Martín L N and Dmitruk P 2013 *Advances in Space Research* **51** 1916–1923
- [19] Cho J and Lazarian A 2009 *Astrophys. J.* **701** 236–252
- [20] Shaikh D 2009 *MNRAS* **395** 2292–2298
- [21] Meyrand R and Galtier S 2013 *Phys. Rev. Lett.* **111** 264501
- [22] Howes G G, Tenbarga J M, Dorland W, Quataert E, Schekochihin A A, Numata R and Tatsuno T 2011 *Phys. Rev. Lett.* **107** 035004
- [23] TenBarga J M and Howes G G 2013 *Astrophys. J. Lett.* **771** L27
- [24] Hatch D R, Jenko F, Bratanov V and Navarro A B 2014 *Journal of Plasma Physics* **80** 531551
- [25] Li T C, Howes G G, Klein K G and TenBarga J M 2016 *Astrophys. J. Lett.* **832** L24
- [26] Passot T, Henri P, Laveder D and Sulem P L 2014 *Eur. Phys. J. D* **68** 207
- [27] Sulem P L and Passot T 2015 *Journal of Plasma Physics* **81** 325810103
- [28] Kobayashi S, Sahraoui F, Passot T, Laveder D, Sulem P L, Huang S Y, Henri P and Smets R 2017 *Astrophys. J.* **839** 122
- [29] Servidio S, Valentini F, Califano F and Veltri P 2012 *Phys. Rev. Lett.* **108** 045001
- [30] Greco A, Valentini F, Servidio S and Matthaeus W H 2012 *Phys. Rev. E* **86** 066405
- [31] Perrone D, Valentini F, Servidio S, Dalena S and Veltri P 2014 *Eur. Phys. J. D* **68** 209
- [32] Valentini F, Servidio S, Perrone D, Califano F, Matthaeus W H and Veltri P 2014 *Phys. Plasmas* **21** 082307
- [33] Servidio S, Valentini F, Perrone D, Greco A, Califano F, Matthaeus W H and Veltri P 2015 *Journal of Plasma Physics* **81** 325810107
- [34] Valentini, F, Vásconez, C L, Pezzi, O, Servidio, S, Malara, F and Pucci, F 2017 *Astron. Astrophys.* **599** A8

- [35] Cerri S S and Califano F 2017 *New Journal of Physics* **19** 025007
- [36] Cerri S S, Servidio S and Califano F 2017 *Astrophys. J. Lett.* **846** L18
- [37] Verscharen D, Marsch E, Motschmann U and Müller J 2012 *Phys. Plasmas* **19** 022305
- [38] Vasquez B J and Markovskii S A 2012 *Astrophys. J.* **747** 19
- [39] Comişel H, Verscharen D, Narita Y and Motschmann U 2013 *Phys. Plasmas* **20** 090701
- [40] Parashar T N, Vasquez B J and Markovskii S A 2014 *Phys. Plasmas* **21** 022301
- [41] Vasquez B J, Markovskii S A and Chandran B D G 2014 *Astrophys. J.* **788** 178
- [42] Hellinger P, Matteini L, Landi S, Verdini A, Franci L and Trávníček P M 2015 *Astrophys. J. Lett.* **811** L32
- [43] Ozak N, Ofman L and Viñas A F 2015 *Astrophys. J.* **799** 77
- [44] Parashar T N, Matthaeus W H, Shay M A and Wan M 2015 *Astrophys. J.* **811** 112
- [45] Parashar T N and Matthaeus W H 2016 *Astrophys. J.* **832** 57
- [46] Franci L, Verdini A, Matteini L, Landi S and Hellinger P 2015 *Astrophys. J. Lett.* **804** L39
- [47] Franci L, Landi S, Matteini L, Verdini A and Hellinger P 2015 *Astrophys. J.* **812** 21
- [48] Franci L, Landi S, Matteini L, Verdini A and Hellinger P 2016 *Astrophys. J.* **833** 91
- [49] Franci L, Landi S, Verdini A, Mattini L and Hellinger P 2017 *ArXiv e-prints* 1711.02664
- [50] Chen C H K, Bale S D, Salem C S and Maruca B A 2013 *Astrophys. J.* **770** 125
- [51] Chen C H K and Boldyrev S 2017 *Astrophys. J.* **842** 122
- [52] Chen C H K, Boldyrev S, Xia Q and Perez J C 2013 *Phys. Rev. Lett.* **110** 225002
- [53] Cerri S S, Franci L, Califano F, Landi S and Hellinger P 2017 *Journal of Plasma Physics* **83** 705830202
- [54] Franci L, Hellinger P, Matteini L, Verdini A and Landi S 2016 *American Institute of Physics Conference Series (American Institute of Physics Conference Series vol 1720)* p 040003
- [55] Franci L, Cerri S S, Califano F, Landi S, Papini E, Verdini A, Matteini L, Jenko F and Hellinger P 2017 *Astrophys. J. Lett.* **850** L16
- [56] Hellinger P, Landi S, Matteini L, Verdini A and Franci L 2017 *Astrophys. J.* **838** 158
- [57] Matthews A P 1994 *J Comput Phys* **112** 102 – 116 ISSN 0021-9991
- [58] Boris J P 1970 *Proceeding of Fourth Conference on Numerical Simulations of Plasmas*
- [59] Qin H, Zhang S, Xiao J, Liu J, Sun Y and Tang W M 2013 *Phys. Plasmas* **20** 084503